Title

Larger cerebral cortex is genetically correlated with greater frontal area and dorsal thickness

Journal

Proceedings of the National Academy of Sciences of the United States of America, 120(11)

ISSN

0027-8424

Authors

Makowski, Carolina
Wang, Hao
Srinivasan, Anjali
et al.

Publication Date

2023-03-14

DOI

10.1073/pnas.2214834120

Peer reviewed

PNAS RESEARCH ARTICLE | NEUROSCIENCE

Larger cerebral cortex is genetically correlated with greater frontal area and dorsal thickness

Carolina Makowski[a,1], Hao Wang[a], Anjali Srinivasan[a], Anna Qi[a], Yuqi Qiu[b], Dennis van der Meer[c], Oleksandr Frei[c], Jingjing Zou[d], Peter M. Visscher[e], Jian Yang[f], and Chi-Hua Chen[a,1]

Edited by Pasko Rakic, Yale University, New Haven, CT; received August 30, 2022; accepted January 18, 2023

Human cortical expansion has occurred non-uniformly across the brain. We assessed the genetic architecture of cortical global expansion and regionalization by comparing two sets of genome-wide association studies of 24 cortical regions with and without adjustment for global measures (i.e., total surface area, mean cortical thickness) using a genetically informed parcellation in 32,488 adults. We found 393 and 756 significant loci with and without adjusting for globals, respectively, where 8% and 45% loci were associated with more than one region. Results from analyses without adjustment for globals recovered loci associated with global measures. Genetic factors that contribute to total surface area of the cortex particularly expand anterior/frontal regions, whereas those contributing to thicker cortex predominantly increase dorsal/frontal-parietal thickness. Interactome-based analyses revealed significant genetic overlap of global and dorsolateral prefrontal modules, enriched for neurodevelopmental and immune system pathways. Consideration of global measures is important in understanding the genetic variants underlying cortical morphology.

genomics | structural MRI | genome-wide association studies | population genetics | fronto-parietal cortex

Significance

Adjusting vs. retaining global measures in analysis of brain MRI data has been a long-standing question and can have important implications for genomic studies of the cortex. Adjusting for global measures ensures that results for regions of interest are not confounded by overall larger brain size. However, adjusting for globals may throw away important signal when total and regional measures are correlated. We show that retaining vs. adjusting for global brain measures in genomic studies impacts gene discovery, particularly for fronto-parietal cortex. Understanding the genetic factors that contribute to expanded association areas in the human brain, such as the prefrontal cortex, can help provide mechanistic insight into higher human cognition and its unique development compared to other species.

The human cerebral cortex has undergone an extraordinary expansion compared to other mammalian species, mirroring the development of many complex traits unique to modern-day humans. The cerebral cortex is a layered, folded sheet of gray matter, and its size can be measured by surface area tangentially and thickness radially, with differential neurodevelopmental programs shaping and regulating these two cortical measures (1). The product of these two measures roughly corresponds to measures of cortical volume (2). Surface area expansion in humans, particularly in functionally unique association areas, has undergone a 2,000-fold increase relative to mice, compared to an only threefold increase in cortical thickness (3). The prefrontal cortex in particular may have disproportionately expanded in humans compared to non-human primates (4). Evidence for disproportionate scaling of prefrontal surface area with total brain size has also been shown through in vivo MRI within humans, particularly in youth (5). Motivated by this latter study and findings of cortical expansion observed across species, here we study phenotypic variation of the cortex captured by genetic information in humans. Differentiating between the genetic variants linked to regionalization and global size of the cortex in humans may give us insights into the functional specialization required in development to define unique brain regions that are important to our understanding of cognition and brain disorders.

Shared genetic influences between local and global measures of cortical anatomy are suggested by neuroimaging studies of genetic disorders and twins. For example, genetic conditions, such as large mutations caused by copy number variants (CNVs), have quite profound effects on both global and regional brain morphology and contribute to several neurodevelopmental conditions (6). Similarly, quantitative genetic analyses obtained from twin-based heritability estimates have suggested genetic overlap between regional surface area/thickness and global measures (7). However, it is unknown which genetic variants contribute to this overlap and how these genetic variants shape global and regional brain development. A study by Shin et al. began to address this question of the different information that can be gleaned from the genetic architecture of global compared to regional features of the cortex, where they carried out genome-wide association studies (GWAS) in 23,000 individuals on the top two principal components of cortical surface area data (8). As expected, the first principal component largely captured global features of the cortex, whereas the second principal component captured occipital/visual cortex-specific surface area. According to this study, the genetic architecture of the first two principal components differentially associated with complex traits, such that the first "global" component seemed to map onto the genetic architecture of general cognitive and learning ability, whereas the second "regional" occipital component had higher genetic correlations

Author contributions: C.M., H.W., P.M.V., J.Y., and C.-H.C. designed research; C.M. and C.-H.C. performed research; C.M., H.W., A.S., A.Q., Y.Q., D.v.d.M., O.F., J.Z., and C.-H.C. processed and analyzed the data; A.S., A.Q., and D.v.d.M. helped with data visualization; C.M., H.W., A.S., A.Q., Y.Q., D.v.d.M, O.F., J.Z., P.M.V., J.Y., and C.-H.C. revised the manuscript; and C.M. and C.-H.C. wrote the paper.

The authors declare no competing interest.

This article is a PNAS Direct Submission.

[1]To whom correspondence may be addressed. Email: cmakowski@ucsd.edu or chc101@ucsd.edu.

This article contains supporting information online at https://www.pnas.org/lookup/suppl/doi:10.1073/pnas.2214834120/-/DCSupplemental.

Published March 9, 2023.

with psychiatric disorders. It remains to be seen how the genetic architecture of global surface area compares and contrasts with other regions of the brain, particularly association cortical regions subserving complex or higher cognitive function (e.g., executive function, memory). Additionally, cortical thickness also shows unique regionalization patterns which shape the functional boundaries of the brain (9).

In this study, we assessed the relationship between global measures (e.g., total surface area and mean cortical thickness across the brain) and regional patterns of genetically informed brain morphology, where brain regions were defined by hierarchical clustering of twin data as presented by our group previously (10–12). The genetically informed brain parcellations applied to this study adhere to known genetic patterning of the cortex, including anterior/posterior and dorsal/ventral developmental axes of surface area and cortical thickness, respectively. To do so, we compared genetic variants and genes associated with 12 surface area and 12 cortical thickness regions from two sets of GWAS, with and without adjustment for global brain measures. Global adjustment is typically done in brain imaging studies to account for the fact that some individuals will have larger morphological features simply due to having a larger brain. We employed an interactome-based gene mapping approach to investigate the genetic overlap or separation in genes associated with global measures and different brain regions. Rather than the traditional approach of focusing on individual genes, network approaches focus on genes in the context of their molecular interactions (interactome) that may more realistically reflect complex biological pathways of polygenic traits (13). We expect that global measures will have higher genetic overlap with association areas (e.g., prefrontal cortex) compared to primary sensory cortices (e.g., occipital cortex), given the disproportionate expansion of association regions that contribute to the protracted course of human brain development and, in turn, higher cognitive function.

Results

Sample. Our discovery sample included brain imaging and genetic data from 32,488 individuals (mean age = 64.2 [range: 45.1 to 81.8, SD: 7.5], %female=52.2) from the UK Biobank. We also included a sample of 9,136 children from the Adolescent Brain Cognitive Development (ABCD) Study® to assess generalizability of our findings. See Dataset S1 for demographics and descriptives of the regional brain data.

GWAS Analyses and Workflow. Twelve regions of interest were extracted per hemisphere based on two genetically informed atlases for cortical thickness and surface area. These atlases have been previously developed by our group (10, 11), using a data-driven fuzzy clustering technique to identify parcels of the human cortex that are maximally genetically correlated based on the MRI scans of over 400 twins.

All GWAS analyses were carried out on pre-residualized brain phenotypes, adjusted for age, sex, scanner site, a proxy of scan quality (FreeSurfer's Euler number) (14), presence of a brain disorder, and the first 10 genetic principal components. See *SI Appendix, Supplementary Methods and Results Materials and Methods* for more details. We denote one set of analyses as GWAS*r* for regional associations, which also adjusts for global measures (i.e., total surface area, mean whole brain thickness) in the pre-residualized regional brain phenotypes, and the second set of regional associations as GWAS*g+r*, which includes global measures (i.e., does not adjust for globals). We also include GWAS of global measures (i.e., total cortical surface area, mean whole brain cortical thickness), which we denote as GWAS*g*. Thus, in total we analyzed 50 GWAS (24 GWAS*g+r*, 24 GWAS*r*, 2 GWAS*g*). See Fig. 1*A* for a visualization of these different GWAS analyses.

Global Measures are Significantly Associated with Regional Phenotypes. We first estimated the effects of the two global measures and chosen covariates (age, sex, scanner, brain diagnosis, Euler number, 10 PCs) on our cortical phenotype data using four sets of tests. See *SI Appendix, Supplementary Methods and Results Materials and Methods* for more details on these tests. AIC and BIC values were both smaller across all phenotypes in the full model compared to the reduced model which excluded global measures, suggesting that the full model including global surface area/thickness provided a significantly better fit to the cortical phenotype data. ANOVA F tests provided a similar conclusion, where the null hypothesis that the simpler (reduced) model is as good as the full model was rejected for all phenotype models. Finally, Least Absolute Shrinkage and Selection Operator (LASSO) consistently selected the global measures as an important contributor to our models for each cortical phenotype. We also ran LASSO easing restrictions and allowing the operator to select from all other 15 covariates in the model. This approach showed that age, sex, and the Euler number (a proxy of image quality) were important contributors to our models for nearly all cortical phenotypes, and scanner contributed notably to about half of the phenotypes. See Dataset S2.

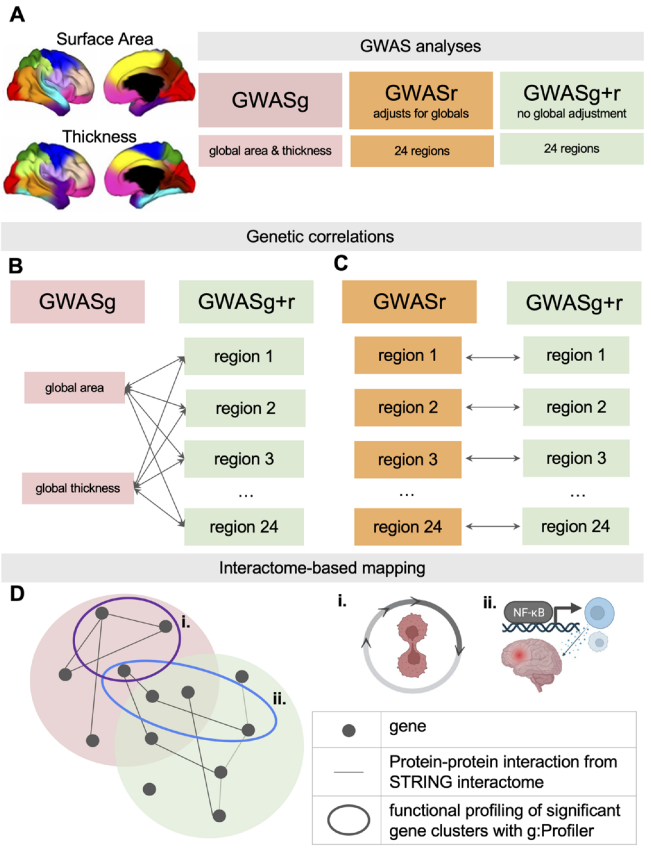

Fig. 1. Methods workflow. *Panel A*: Three sets of GWAS on GWAS of global measures (GWASg), GWAS of 24 brain regions adjusting for global measures (GWASr) and GWAS of 24 brain regions not adjusting for global measures (GWASg+r). *Panels B and C*: Two sets of genetic correlation analyses with LDSC. *Panel D*: Interactome-based mapping of gene lists comparing GWASg and GWASg+r phenotypes. For select phenotype pairs, functional profiling was then carried out with g:Profiler for functional interpretation of meaningful gene clusters within the Venn Diagram, for example *i*. cell cycle-related annotations; *ii*. inflammatory pathways, such as processes involving Nuclear Factor Kappa B (NF-κB).

GWAS of Cortical Phenotypes for both GWAS*r* and GWAS*g+r*. We compared the number of significant loci associated with our cortical phenotypes for GWAS*r* (Datasets S3 and S4) and GWAS*g+r* (Datasets S3 and S5). In our latest work on the same sample (12), we reported 393 significant loci associated with our 24 cortical phenotypes, after clumping with PLINK (15) ($r^2 = 0.1$, distance = 250 kb) and thresholding at $P < 5e\text{-}8$, of which 361 loci had unique rsIDs (i.e., 8% duplicated loci). Further, for GWAS*g* we found 27 and 20 variants significantly associated with total cortical surface area and mean cortical thickness, respectively. For GWAS*g+r*, we obtained 756 significant loci across the 24 cortical phenotypes, of which 419 were unique; in other words, 45% were duplicated loci with the same rsIDs, due to the recounting of loci underlying global measures. Significant loci from GWAS*g* that were also associated with multiple brain regions are listed in Dataset S6. Across the unique genome-wide significant loci for GWAS*r* and GWAS*g+r*, 267 and 225 were found to be LD-independent by clumping all phenotypes together in PLINK (15) ($r^2 = 0.1$, distance = 250 kb). Miami plots comparing these two GWAS approaches, as well as number of hits per region, can be found in Fig. 2 *A* and *B* for area and thickness, respectively.

Extending our previous work to assess generalizability of results from GWAS*r* to an independent sample (12), we also incorporated a neurodevelopmental sample of diverse ancestry using ABCD Study data. We show that the majority of genome-wide significant SNPs from our discovery cohort are still significant after including ABCD Study participants in a meta-analysis (Dataset S7). We also found high correspondence between samples as indexed by sign concordance rate (GWAS*r*: 0.93, $P < 2.2e\text{-}16$; GWAS*g+r*: 0.88, $P < 2.2e\text{-}16$; GWAS*g*: 0.86, $P = 7.43e\text{-}06$). The proportion of significant SNPs from the UK Biobank (UKB) sample that remained significant at $P < 0.05$ were as follows for the three GWAS methods: GWAS*r* proportion: 0.57, $P = 0.0097$; GWAS*g+r*: 0.41, $P = 3.03e\text{-}05$; and GWAS*g*: 0.30, $P = 0.02$.

Gene set analysis results for both GWAS*r* and GWAS*g+r* can be found in Fig. 3 *A* and *B*, respectively (Datasets S8 and S9). Gene set analysis with GWAS*g+r* revealed additional terms, particularly for surface area, related to cancer pathways (which can also be interpreted as pathways linked to canonical cell cycle pathways), neurogenesis, and longevity, that were not found in GWAS*r*. Additionally, the cancer-associated terms were also associated with the GWAS*g* results of total surface area. Many of these enrichments remained significant after filtering the background gene sets for genes expressed in the brain based on the Human Protein Atlas (16), suggesting many of the biological pathways uncovered are specific to brain tissue. SNP-based heritability range estimates from LDSC are as follows and can be found in Dataset S10: GWAS*r*, area from 0.23 to 0.36; GWAS*r*, thickness from 0.15 to 0.25; GWAS*g+r*, area from 0.35 to 0.39; GWAS*g+r*, thickness from 0.21 to 0.31. Consistent with previous work, after regressing out globals, heritability estimates significantly drop on average by 0.09 (25.3%) and 0.07 (25.6%) for area and thickness, respectively. This can be compared to a drop of ~0.2 (50%) and ~ 0.1 (27%) using twin heritability estimates (7).

As has been shown previously (8, 17), we observed large effects in global surface area for loci within the 17q21.31 inversion region. This signature on chromosome 17 was seen across all 12 surface area phenotypes for GWAS*g+r* analyses but not for

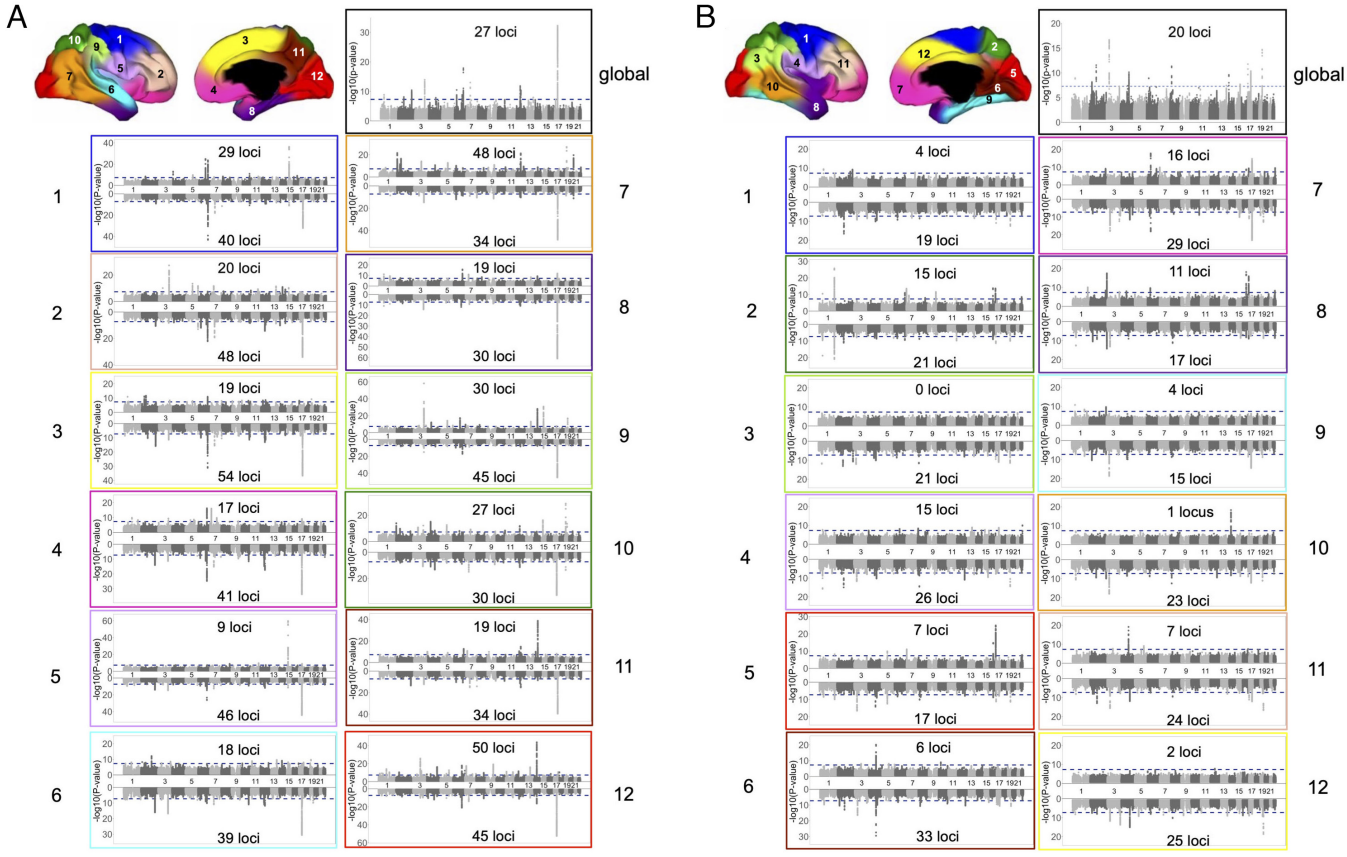

Fig. 2. Miami plots colored by atlas region for *Panel A.* surface area and *Panel B.* cortical thickness. Top half of Miami plot for GWAS*r* and bottom half for GWAS*g+r*. Manhattan plots for global surface area and mean cortical thickness are included in the top right of each panel. A number of significant loci (defined by plink, $r^2 = 0.1$, 250 kb) for each analysis are included in each subplot. Numeric and colored labels on brain maps correspond to the same number/color of each subplot.

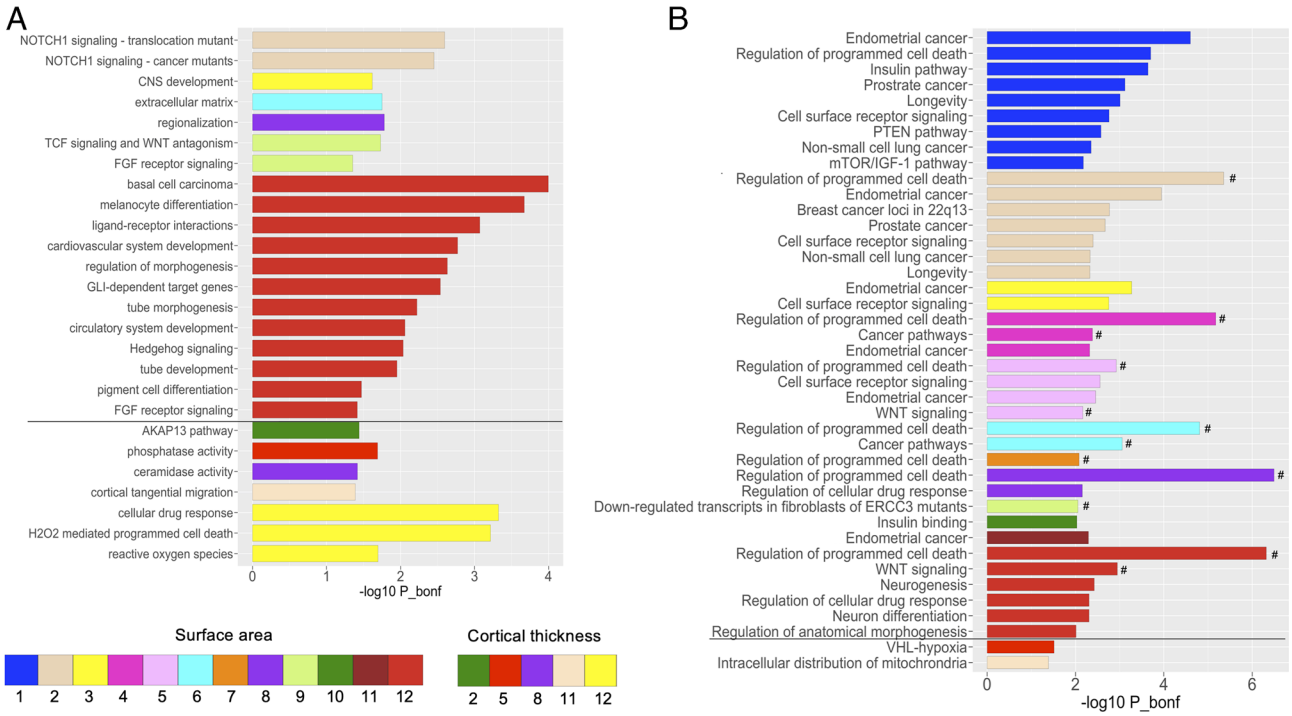

Fig. 3. Bonferroni-corrected terms from gene set analysis ($P < 0.05$, unless otherwise specified) for *Panel A*. GWAS*r* (adapted from ref. 12) and *Panel B*. GWAS*g+r*. Bars are color-coded by cortical region, where the region numbers included in the legend correspond to region numbers in Fig. 2. Results above the horizontal black line represent surface area regions and regions below for cortical thickness. Hashtags (#) in *Panel B* reflect terms that are also significantly associated with global surface area. For readability, only terms with Bonferroni-corrected $P < 0.01$ are displayed in *Panel B*. See full list of Bonferroni-corrected terms ($P < 0.05$) in Dataset S9.

GWAS*r*, emphasizing the additional signal that global brain measures offer in detecting genetic loci shaping the brain. The most significant loci associated with any particular region also varied by approach; for GWAS*r*, the strongest signal was detected for rs7182018 (P = 2.2e-60, variance explained 0.83%) associated with pars opercularis area within 15q14; for GWAS*g+r*, rs55751924 (P = 1.33e-61, variance explained 0.84%) associated with anteromedial temporal area on 17q21.31; and for GWAS*g*, rs593720 (P = 4.94e-33, variance explained 0.44%) associated with total surface area also within 17q21.31. Intriguingly, we did not see a strong signal on 15q14 associated with global area, despite its contribution to the surface area of pars opercularis of the inferior frontal cortex. For mean cortical thickness, the strongest association was found with rs694611 (P = 2.10e-17, variance explained 0.22%) on chromosome 3, a genetic locus that was also found to be significantly associated with the thickness of most phenotypes in GWAS*g+r*. This SNP lies within the *RPSA* gene, which has recently been shown to have an important role in early cortical development, particularly for dendritic spine morphology and cortical layering (18).

Comparing Genetic Architectures to quantitatively assess the Contribution of Global Measures.

Comparing GWAS$_g$ with GWAS$_{g+r}$. We calculated LD score regression (LDSC)-based genetic correlations (rg) between GWAS of each global measure (GWAS*g*: total surface area and mean thickness) and GWAS*g+r* results for the 24 cortical phenotypes to better understand the contribution of global measures to regional brain morphology (Fig. 1*B*). As can be seen in Fig. 4*A*, the highest genetic and phenotypic correlations with global area were found with anterior/frontal regions; and for global thickness, highest correlations were with dorsal regions, specifically fronto-parietal (rg and phenotypic correlation ranges, respectively, for i) global area with regional area: 0.80 to 0.93, 0.82 to 0.92; ii) global thickness with regional thickness 0.71 to 0.92, 0.69 to 0.88; all P's < 4e-4) (Fig. 4*A* and Dataset S11). We also ran this genetic correlation analysis for a subsample of the ABCD dataset (N = 5,360 of predominantly European ancestry) (Dataset S11), finding similar trends in genetic correlations (e.g., highest correlations between total surface area and anterior regions and lowest for occipital area). Note the small sample size of ABCD yields more noise in genetic correlation estimates, thus cautious interpretation is warranted. *SI Appendix*, Fig. S1 shows the genetic and phenotypic correlations between global area and regional thickness (rg range: −0.20 to −0.55; phenotypic r range: −0.08 to −0.39) and global thickness and regional area (rg range: −0.26 to −0.36; phenotypic r range: −0.08 to −0.20; all P's < 4.e-4). There was strong correspondence between corresponding genetic and phenotypic correlations (*SI Appendix*, Fig. S2).

Comparing GWAS$_r$ and GWAS$_{g+r}$ results. We also used LDSC to compute genetic correlations between GWAS*r* and GWAS*g+r* results for each of the 24 brain regions as another way of understanding and visualizing the genetic contributions of global measures to regional brain morphology. Genetic correlation results can be found in Fig. 4*B* and Dataset S10, where we find genetic correlations between GWAS*r* and *GWAS*g+r of the same phenotypes range from 0.26 to 0.57 for surface area and 0.39 to 0.69 for cortical thickness (mean rg: 0.49, mean SE: 0.042, all P's < 4e-7). Generally, there were higher genetic correlations for cortical thickness compared to surface area, and higher associations were found for primary sensory/motor regions compared to association cortex and frontal regions. This approach gave expected results, with a reversal of patterns shown in the section above. For example, of the area phenotypes, occipital area has the highest rg between GWAS*r* and GWAS*g+r* but lowest rg between GWAS*g* and GWAS*g+r*, suggesting that occipital area is least affected by adjustment for total surface area. In other words, genetic factors that influence occipital area are less similar than those that influence total surface area.

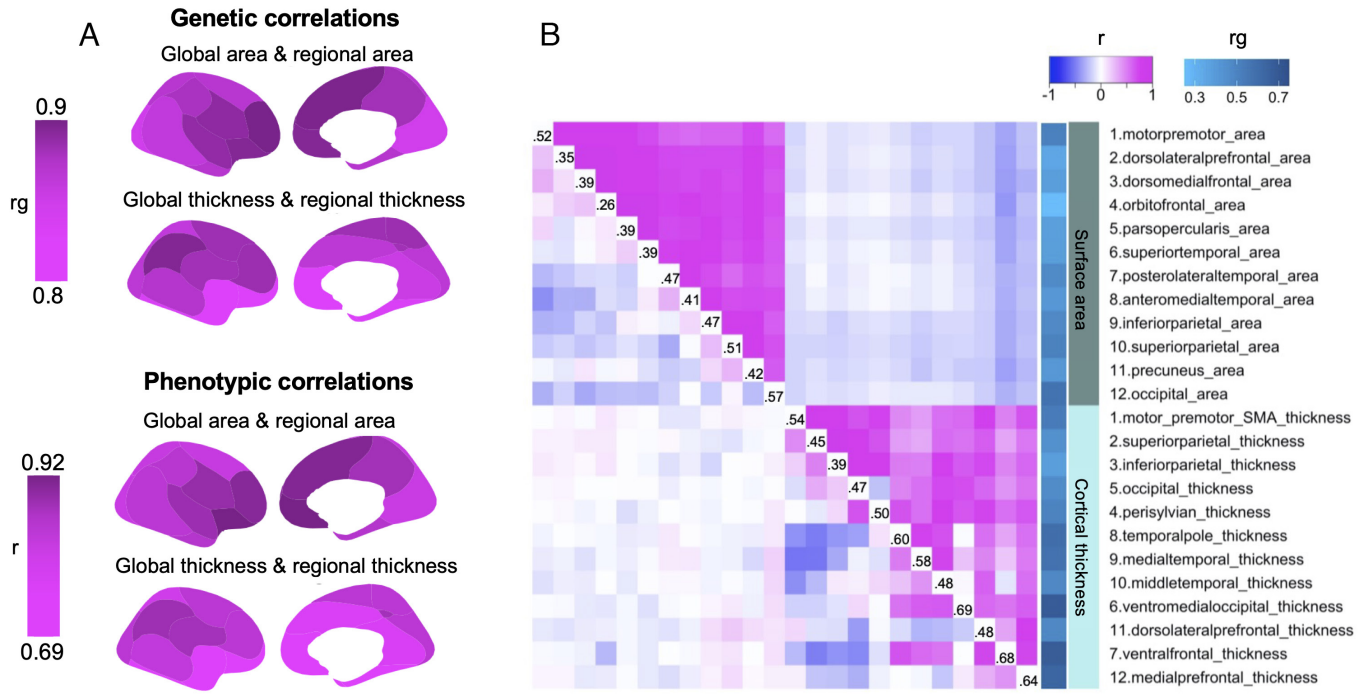

Fig. 4. Phenotypic and genotypic relationships. *Panel A*: Genetic (top two rows) and phenotypic (bottom two rows) correlations between global measures (GWAS*g* for genetic correlations) and regional measures not adjusting for global measures (GWAS*g+r* for genetic correlations). *Panel B*: Lower triangle of matrix displays phenotypic correlations when globals are regressed out, whereas upper triangle shows phenotypic correlations when globals are *not* regressed out during pre-residualization. The diagonal labels reflect genetic correlations between GWAS*r* and GWAS*g+r* results, which are also depicted in the blue color bar to the right of the matrix.

For completeness, we also looked at the phenotypic correlations between all 24 regions comparing GWAS*r* and GWAS*g+r*, which can be found in Fig. 4*B*. We have previously published the phenotypic correlations for GWAS*r* (11, 12, 19). Notably, much more uniform phenotypic correlation structures emerge when globals are not regressed out, likely due to the shared global genetic variants underlying many regions. Specifically, we observe largely positive correlation structures within a trait (e.g., one area region with another area region), but negative correlations across traits (e.g., one area region with a thickness region) (Fig. 4*B*).

Overlap in Genetic Modules between Global and Regional Brain Measures. We carried out a network separation analysis adapted from Menche et al. (20) to see whether the genes underlying global measures (i.e., from GWAS*g*) were overlapping or separated from genes underlying regional brain measures (i.e., from GWAS*g+r*). This network approach was motivated by the idea that genes of polygenic traits do not operate in isolation, but in combination and interaction with other genes. We harnessed data from a protein–protein interaction network or "interactome" present in the STRING database (21) and define genetic modules based on the premise that protein products of genes that are associated with a particular trait tend to interact with each other and converge on related biological and functional networks, rather than being randomly spread throughout the interactome (20, 22). We assessed the degree of overlap in genetic modules from GWAS*g* compared to GWAS*g+r* by calculating separation (S_{AB}) and mean shortest distance (d_{AB}) between each global (A) and regional brain region (B) pair. Calculations for these metrics are outlined in *Materials and Methods.*

We used Multi-marker Analysis of GenoMic Annotation (MAGMA) to define genes included in the genetic modules for global and regional phenotypes. SNPs were selected that were within exonic, intronic, and untranslated regions as well as SNPs within 50 kb upstream and downstream of the gene, a window size that has been used in previous cortical GWAS (17). A summary of associated MAGMA genes is included in Dataset S12, and lists of genes and statistics are found in Datasets S13 and S14 for GWAS*r*, GWAS*g*, and GWAS*g+r*. Consistent with the genetic correlation patterns, genetic modules between global and regional phenotypes, for both area and thickness, showed significant overlap, as demonstrated by negative separation values (sAB z-scores, area range: −3.84 to −14.70; thickness range: −4.13 to −14.51; all p's < 2e-5). See Dataset S15 for separation and shortest distance statistical results. Overlap in genetic modules was particularly high between global area and area of prefrontal regions (e.g., orbitofrontal, pars opercularis), as well as between global thickness and thickness of fronto-parietal regions (e.g., dorsolateral prefrontal, inferior parietal), consistent with genetic correlation results presented in Fig. 4*A*. Genes that were mapped by MAGMA but not found in the STRING interactome database are excluded and listed in Dataset S16; the function of many of these excluded genes remains largely unknown as they are pseudogenes or non-coding RNA genes. The genetic overlap between global (GWAS*g*) and regional measures (GWAS*g+r*) is displayed for two exemplary pairs in Fig. 5: i) global surface area and dorsolateral prefrontal area and ii) global thickness and dorsolateral prefrontal thickness. Functional profiling of gene lists from each separate module (e.g., brain region) and overlapping genes was completed with g:Profiler (23) and revealed many overlapping genes were important in immune function and early neurodevelopmental processes. Network figures were created using Cytoscape (24) (Fig. 1*D*).

In addition to using gene lists generated by MAGMA, we also computed separation statistics using genes mapped by Functional Mapping and Annotation of Genome-Wide Association Studies (FUMA), which includes intergenic mapping (Datasets S18–S20). On average, about 55% of MAGMA genes were found to be overlapping with the FUMA mapped genes, where the lowest

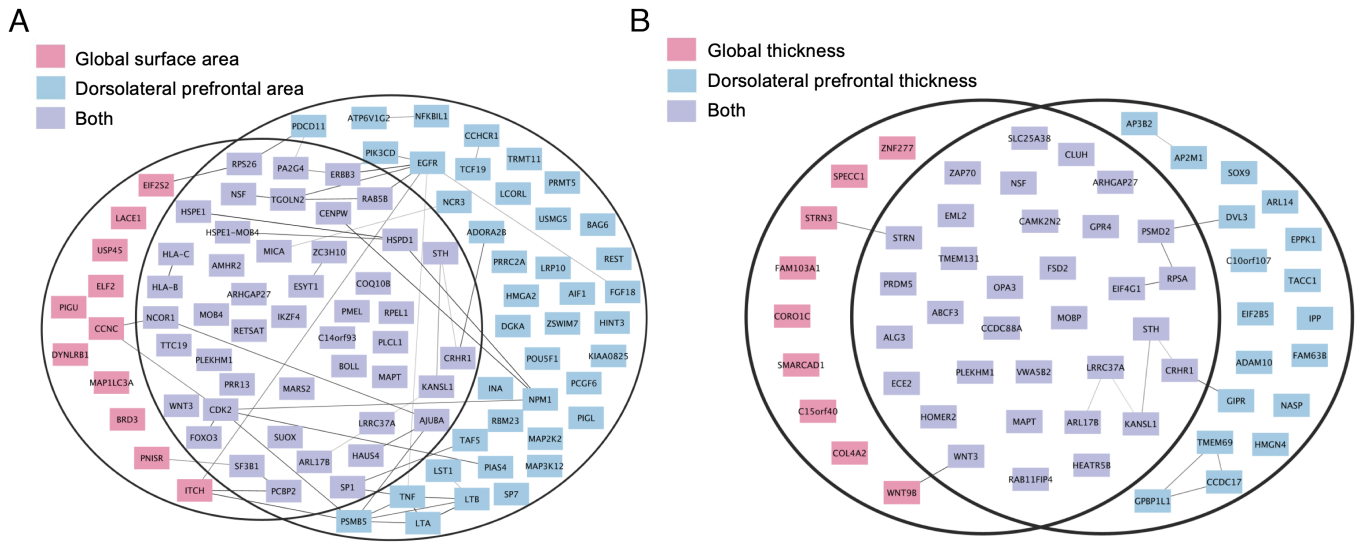

Fig. 5. Venn Diagrams of overlap in genetic modules for two exemplary pairs. *Panel* A: global surface area and dorsolateral prefrontal cortical area, and *Panel B:* global thickness and dorsolateral prefrontal thickness. Nodes in the graph represent genes, and edges (gray lines) represent connections between genes as defined by the STRING interactome.

overlap was found for pars opercularis area with 11.1% overlap and the highest for motor-premotor thickness with 84.5% overlap (Dataset S21). Of these overlapping genes, on average 66% of genes were identified through positional mapping in FUMA. Although there is no complete overlap between MAGMA and FUMA gene lists, our separation results yield similar results and interpretation across both gene mapping methods (Dataset S15).

Finding Common Genetic Loci between the Two Sets of Analyses. In addition to assessing overlap in genetic modules between traits with an interactome-based mapping approach, we also compared the list of significant loci (clumped with PLINK (15) with $r^2 = 0.1$, distance = 250 kb, $P < 5e\text{-}8$) between GWAS*r* and GWAS*g+r*. We first identified common SNPs based on shared rsID by region, which identified 31 SNPs. Given that significant SNPs in LD with the identified SNPs may also be shared between analyses, we also proceeded to use conditional and joint (COJO) analysis (25) of GWAS summary statistics implemented in Genome-wide Complex Trait Analysis (GCTA) to map shared SNPs for each cortical phenotype. We defined SNPs as being shared between the two approaches as those that were no longer genome-wide significant (i.e., $P > 5e\text{-}8$) in GWAS*g+r* when conditioned on the significant loci defined by the GWAS*r* analysis of region *k*. There were 70 SNPs identified through this approach, signifying the most "regional" SNPs, which were mapped to genes involved in immune-related pathways and cellular function. These SNPs are presented in Dataset S17, and associated gene set results in *SI Appendix*, Fig. S3. As an additional approach to quantifying overlap between the three GWAS methods (GWAS*r*, GWAS*g+r*, and GWAS*g*), we compared lists of SNPs which included those in high LD ($r^2 > 0.8$) within 5 Mb of the main genome-wide significant SNPs for each of the area and thickness phenotypes (*SI Appendix*, Figs. S4 and S5). These results show patterns of both unique and overlapping genetic variants across methods underlying all regions and highlight in particular larger overlap between anterior/frontal regions and global surface area.

Sensitivity Analyses. To ensure our genetic correlation estimates were not biased by the inclusion of a given region of interest in our global measure, we estimated the genetic correlation between GWAS*g+r* for dorsolateral prefrontal area and GWAS*g* for a modified global surface area measure where we excluded dorsolateral prefrontal area from the calculation. Results were highly similar (rg between dorsolateral prefrontal and original global measure: 0.93 [s.e.: 0.013]; rg between dorsolateral prefrontal and modified global measure excluding dorsolateral prefrontal area: 0.91 [s.e.: 0.0093]). Finally, to address the possibility that some regions scale nonlinearly with the global brain measure, we re-ran all GWAS*r* after log-transforming both the regional and global measures. Across the 24 regions, we found that genetic correlations between these newly generated log-transformed results and our original results approximated 1 (Dataset S22). Given the very high genetic overlap between the two methods, we can conclude that our original approach of treating global measures as a linear covariate is appropriate for our research question.

Discussion

This work shows the importance of considering global cortical measures in understanding the genetic variants underlying cortical morphology. Total surface area and mean cortical thickness are important contributors to phenotypic variation across all 24 brain phenotypes as identified by various statistical model fits, including LASSO. We show that human cortical area expansion is most associated with anterior/frontal expansion, and thicker cortex is most associated with dorsal/fronto-parietal thickening across individuals. The lowest genetic overlap was found between total surface area and occipital area, concordant with previous reports using transcriptome data in humans (26, 27) and non-human primates (28) to show that the genetic patterning of the visual cortex is most distinct from other cortical regions. Given the higher genetic overlap we found between global measures and association cortex (e.g., fronto-parietal regions), we investigated this further with a database of protein–protein interactions to understand the biological pathways that may contribute to the unique expansion of brain regions subserving cognitive functioning. Our interactome-based approach highlights the important information that can be gleaned from looking at the interactions between gene products rather than individual gene lists to assess shared genetic architecture and, in turn, shared biological mechanisms, between two traits. Further, mapping such gene networks and their interactions can help us pinpoint specific functional modules that are

important in understanding and treating neuropsychiatric disorders (22, 29, 30). Finally, our study harnesses the strengths of using genetically informed cortical atlases (10, 11, 31), where we have shown that area measures of these cortical regions have higher heritability and discoverability compared to other atlases in previous work (12, 32). These genetically informed atlases represent a parsimonious set of cortical genetic regions or units that can be confidently defined given the current spatial resolution of MRI, as the boundaries and number of regions were data-driven and entirely determined by clustering algorithms. These cortical regions are relatively large compared to other atlases but still remain biologically plausible given that arealization is primarily genetically determined by signaling molecules and morphogens, which show a large spatial distribution in animal models (1, 33).

Our work highlights both pros and cons for the use of global measures in GWAS models. The benefits of adjusting for global brain measures allow us to identify variants associated with regional measures relative to global measures. On the other hand, adjusting for global measures may reduce signals of interest, especially for regions such as the prefrontal cortex that are highly genetically correlated with global measures. Indeed, the strong impact of global brain measures on regional brain results has been demonstrated in association with many copy number variants (6), which some of our common variants may also tag. Adjustment for global measures may also introduce a potential collider bias in the case that global measures along with genetic variants directly affect regional morphology (34); exploration of more complex statistical models to capture the potential bidirectional relationship between regional and global cortical morphology is warranted in future studies.

Many of the overlapping genes that were linked to both global and regional brain measures seem to be important in regulating immune function. The immune system has increasingly been recognized as a key player in early brain development (35, 36). In particular, the convergence of neurodevelopmental and immune function processes in brain regions with protracted developmental trajectories (e.g., prefrontal cortex) (37, 38) may help us contextualize our results of the genetic mechanisms contributing to the unique expansion of these brain regions. Indeed, we found genes involved in immunoregulation to be shared between surface area of the brain globally and dorsolateral prefrontal cortex regionally, such as the NF-κB pathway which responds to brain injury but also plays a role in brain plasticity and neurogenesis (39). The role of the immune system, particularly microglia and other cytokines, in early prefrontal cortical development is thought to be important in shaping excitatory/glutamatergic neural circuits, where disruptions can confer later vulnerability to known neurodevelopmental disorders such as autism and schizophrenia (40). We also found overlapping genes between global area and dorsolateral prefrontal cortex involved in GABAergic signaling, and for the growth factor receptor *EGFR*, which plays an important role in maintaining the progenitor pool in early brain development at a time when both neuronal and glial cells are being generated (41). The functional profiling of these overlapping genes is consistent with the hypothesis that immune genes involved in prefrontal cortical development contribute to synaptic pruning and myelin growth events (42).

Shared genes (e.g., *EIF4G1*, *PSMD2*, *RPSA*, *WNT3*, *WNT9B*) between global thickness and dorsolateral prefrontal thickness revealed an intriguing overlap in processes involved in Slit/Robo and WNT signaling, important for axon guidance and anterior/posterior patterning of the cortex, respectively (1, 43). Collectively, these genes were also tied to molecular processes of dopaminergic differentiation, which provides an additional layer of evidence that may help contextualize our finding from gene set analyses suggesting enrichment for genes involved in tangential migration underlying dorsolateral prefrontal thickness.

Our results showcase how adjusting for global brain measures in GWAS models can change the interpretation of the biological pathways underlying regional brain morphology. Our gene set analyses exemplify this, with common and unique biological processes associated with each region between the two GWAS approaches. Notably, the common processes are related to neurodevelopment. On the other hand, we find a large proportion of gene set terms associated with cancer and cell signaling pathways underlying many of our brain phenotypes in GWAS analyses that retain the global signal (e.g., do not adjust for global measures), which overlaps with the gene set terms enriched for global surface area (indexed by hashtags # in Fig. 3*B*). Several genes contributed to these cell signaling pathways, which are also observed in databases related to cancer, such as *FOXO3, PIK3CD, AKT3,* and *TCF7L1*. These genes are relevant to neurodevelopment as they are involved in general cell cycle maintenance processes, such as *TCF7L1* for regulation of cell cycle genes (44), and *PIK3CD* playing a role in signaling cascades involved in cell growth, survival, and proliferation (45).

Our findings also highlight the importance of studying inversion polymorphisms, particularly on 17q21.31, when mapping brain morphology. Consistent with Shin et al.'s GWAS findings of the first principal component explaining a large proportion of variance in surface area data (8), we also found an enrichment of SNPs associated with global surface area located on chromosome 17. Global expansion of the brain and association cortex in early development could be enriched for genes linked to the 17q21.31 inversion region. For instance, we see six shared genes in this inversion polymorphism region between global and dorsolateral prefrontal area (i.e., *SPPL2C*, *MAPT*, *STH*, *KANSL1*, *ARL17B*, *LRRC37A*), which together are involved in morphology of apical dendritic contacts and, in turn, neuronal communication. Four of these six genes show stronger effects (i.e., explain more variance) in dorsolateral prefrontal area compared to global area, supporting the idea that genes in the 17q21.31 inversion region may contribute to the disproportionate expansion of prefrontal cortical regions.

Genetic correlations between global measures and individual brain regions recapitulated cortical hierarchy and complemented our previous work (10–12) and that of others showing disproportionate expansion of association cortical areas with larger brain size (5). We show once again an anterior/posterior gradient of genetic correlations with total surface area and regional area, alongside a dorsal/ventral pattern of correlations with mean cortical thickness and regional thickness. The latter thickness gradient has also been independently demonstrated in a twin study of cortical topological organization (46). Altogether our results suggest the important role of global measures in understanding this known cortical hierarchical structure.

We acknowledge several limitations in our current study. Firstly, we include several covariates in our models that do correlate with global brain measures, namely age and sex. It is well-established that males tend to have larger brain size, thus regressing out sex may contribute to removal of some global effects, even in our GWAS*g+r* models. Including age as a covariate may also have a similar effect, especially for cortical thickness, although the majority of our discovery sample is within an age range that precedes steep declines in cortical thinning, and our results still hold when including a neurodevelopmental sample in a meta-analysis. Secondly, our discovery sample is of European descent, although we have previously shown and demonstrate once again in this

work, that GWAS results largely replicate in a sample of diverse ancestry. Thirdly, we acknowledge that our interpretation of results is impacted by our chosen gene mapping strategy and interactome database selection. The method we used, MAGMA, links genes based on their spatial proximity to a SNP, but may not always be the most relevant gene (47), although there have been reports for specific traits where the likelihood of the nearest gene being causal is high (48). Accurate gene mapping is a challenge in the field of genetics more broadly (49), but we have included results from other gene mapping strategies in our supporting information to offer readers resources from other tools, and found that these alternative mapping strategies provided similar interpretation of results.

Given that many brain imaging and genetics studies of structural brain features regress out global measures (50, 51), this study provides a more nuanced view of how global measures add to our interpretation of the genetics underlying brain morphology. The overlap in genetic architecture between global measures and multiple distributed brain regions could also be further elucidated with multivariate methods in future work, given its success in boosting discovery of novel genetic variants underlying cortical morphology (52–54). Understanding global as compared to regional patterns of cortical morphology can have important implications for our understanding of higher cognitive function (55) and, in turn, psychiatric and neurological disorders that impact such cognitive processes.

Materials and Methods

Sample. Imaging and genomics data were taken from participants of the UK Biobank (UKB) population cohort, obtained from the data repository under accession number 27412 (56–59). All participants gave written informed consent (59). The composition, setup, and data gathering protocols of the UKB have been extensively described elsewhere (56–58). For this study, White Europeans were selected that had undergone the neuroimaging protocol. We excluded individuals with bad structural scan quality as indicated by an age and sex-adjusted Euler number (14) more than three SDs lower than the scanner site mean. Our final sample included 32,488 individuals (mean age = 64.2 [range: 45.1 to 81.8, SD: 7.5], %female = 52.2).

We also conducted an additional analysis to see whether results generalize to a neurodevelopmental cohort. Neurodevelopmental data came from 9 to 10-y-old children from the ABCD Study (abcdstudy.org) (60, 61). The ABCD Study is an ongoing longitudinal multisite study within the United States that is publicly available through the National Institute for Mental Health (NIMH) Data Archive (NDA). Exclusion criteria include 1) lack of English proficiency; 2) presence of severe sensory, neurological, medical, or intellectual issues that would interfere with the child's ability to comply with the protocol; and 3) an inability to complete an MRI scan at baseline. Baseline data from ABCD release 2.0.1 were used. We included all individuals with imaging and genomics data that passed quality control (N = 9,136; mean age = 9.93 [range: 9.0 to 10.9, SD = 0.62], % female: 47.6, % European descent: 58.7, % admixed: 41.3). Each site obtained approval from their Institutional Review Board, and all participants underwent verbal and written consent/assent. All information relevant to the ABCD Study is outlined in *SI Appendix*.

MRI Processing and Atlas Definition. T1-weighted scans were collected from three scanning sites throughout the United Kingdom on identical Siemens Skyra 3T scanners with a 32-channel receive head coil. The UKB core neuroimaging team has published extensive information on the applied scanning protocols and procedures (58). The T1 scans were obtained from the UKB data repositories and stored locally at the secure computing cluster of the University of Oslo. The standard "recon-all -all" processing pipeline of Freesurfer v5.3 was applied to perform automated surface-based morphometry segmentation (62). Both surface area and cortical thickness are defined at the vertex level, with surface area extracted from the white surface, and cortical thickness calculated as the distance between the white surface and pial surface.

Twelve regions of interest were extracted per hemisphere based on two genetically informed atlases for cortical thickness and surface area. These atlases have been previously developed by our group, using a data-driven fuzzy clustering technique to identify parcels of the human cortex that are maximally genetically correlated based on the MRI scans of over 400 twins. No spatial information was used in creating the atlases. The only information used in deriving the parcels was the genetic correlations of cortical thickness or surface area among all vertices. More details can be found in our previous work (10, 11). We combined cortical phenotypes across hemispheres, as we have previously presented (12).

Before running the GWAS on each measure, we regressed out age, sex, scanner site, a proxy of scan quality (FreeSurfer's Euler number) (14), and the first 10 genetic principal components from each measure. We also regressed out whether or not the individual had a brain diagnosis based on ICD10 diagnostic information collected by the UKB (https://biobank.ndph.ox.ac.uk/showcase/field.cgi?id=41202). Individuals were classified as having a brain diagnosis if they met criteria for at least one class F (mental and behavioral disorders) or class G (disorders of the nervous system) diagnosis, with the exception of G56-carpal tunnel syndrome, which is an extremely common condition and thus we did not consider it as a neurological diagnosis. Approximately, 8% of our UKB sample were classified as having a mental/behavioral or neurological disorder. Subsequently, we applied a rank-based inverse normal transformation to the residuals of each measure, ensuring normally distributed input into each GWAS.

We denote one set of analyses as GWAS*r* for regional associations only after adjusting for global measures (i.e., total surface area, mean whole brain thickness) in the pre-residualized phenotypes, and the second set as GWAS*g+r*, which does not adjust for globals (Fig. 1*A*).

Contributions of Global Measures to Model Fits per Phenotype. Four sets of tests were used to compare model fits when including and excluding global measures for our cortical phenotypes. These models all included the 15 covariates outlined above (age, sex, scanner, brain diagnosis, Euler number, 10 PCs). First, the Akaike Information Criterion (AIC) was applied (63). AIC is often used by stepwise variable selection models and estimates the relative amount of information lost by a given model. We then applied the Bayesian information criterion (BIC) (64), which is another criterion for comparing regression models. For both AIC and BIC, the smaller the value, the better the model. Next we used an ANOVA F test, which compares a full model and its reduced model, with the null hypothesis that the simpler (reduced) model is as good as the full model. Finally, we applied the Least Absolute Shrinkage and Selection Operator (LASSO) (65), which uses cross-validation to calculate the mean square error (MSE) for every combination of predictors and then selects the best regression model with the minimum MSE. We first fixed all 15 covariates or predictors, to see if LASSO would select the global variable (mean thickness or total surface area) into the best model. Finally, this restriction was released to allow LASSO to select from all 16 predictors.

Genotype Quality Control and Imputation. The UKB v3 imputed data were used, which has undergone extensive quality control procedures as described by the UKB genetics team (59). After converting the BGEN format to PLINK binary format, additional standard quality check procedures were carried out, including removal of single nucleotide polymorphisms (SNPs) with low imputation quality scores, filtering out individuals with more than 10% missingness, SNPs with more than 5% missingness, and SNPs failing the Hardy-Weinberg equilibrium test at $P = 1*10^{-6}$. A minor allele frequency threshold of 0.01 was used, leaving 7,853,566 SNPs. To further account for population substructure, we used results from UKB-specific principal components analysis (PCA), which were generated with flashPCA (66).

GWAS of Cortical Phenotypes for both GWAS*r* and GWAS*g+r*. We used fastGWA implemented in GCTA (67), a mixed linear model-based tool, that controls for population stratification by principal components and takes into account relatedness using a sparse genetic relationship matrix. This method extends linear mixed model-based association analysis for use of biobank-scale data in a resource-efficient manner. The genome-wide significant loci were defined by clumping in PLINK (15) ($r^2 = 0.1$, distance = 250 kb) and thresholded at $P < 5e\text{-}8$. Hits corrected for multiple comparisons can be found in our previous work (12) and in Dataset S3.

We then computed genetic correlations using LDSC (68) per region between GWAS*g* and GWAS*g+r* (Fig. 1*B*). We also computed genetic correlations per region

between GWAS*r* and GWAS*g+r* summary statistics, where only the former set of GWAS regresses out the global signal (Fig. 1*C*).

Functional Follow-Up with FUMA. We used the web tool Functional Mapping and Annotation of Genome-Wide Association Studies (FUMA) (https://fuma.ctglab.nl/) (69) to conduct a generalized gene set analysis using MAGMA within FUMA (70) to generate gene lists from GWAS*r* and GWAS*g+r* results, as well as gene lists for global area and thickness. For each gene, SNPs were selected that were within exonic, intronic, and untranslated regions as well as SNPs within 50 kb upstream and downstream of the gene, a window size that has been used in previous cortical GWAS (17). We used the 19,241 protein-coding genes in MAGMA in our main analysis. The gene-based *P*-value was calculated based on the mean of the summary statistic (χ^2 statistic) of GWAS for the SNPs in a gene (70). The *P*-value significance threshold was determined using the Bonferroni method, 0.05 divided by the number of genes (19,241), which is 2.6×10^{-6}. The genes for GWAS*r* and the global measures have been previously reported in Makowski et al. (12). Gene set enrichment analysis using MAGMA genes was carried out with 15,485 gene sets from MsigDB v6.2. An additional analysis was carried out filtering the background gene sets for genes expressed in the brain using the Human Protein Atlas (16) (http://proteinatlas.org).

We also used FUMA to annotate significant SNPs from GWAS*r,* GWAS*g,* and GWAS*g+r*, using positional, eQTL, and chromatin interaction mapping. Summaries and details of these gene lists can be found in *SI Appendix* (MAGMA: Datasets S12–S14; FUMA: Datasets S18–S20). Additional information on these three mapping strategies is as follows:

i. Positional mapping of SNPs, whereby SNPs within a 10 kB window from known protein-coding genes in the human reference assembly (GRCh37/hg19) are mapped;
ii. eQTL mapping whereby allelic variations at a SNP are significantly linked to expression of a gene, where we considered eQTLs within cortical structures from GTEx v8, the UK Brain Expression Consortium (http://www.braineac.org/), the Common Mind Consortium (71), and PsychENCODE (72) (http://resource.psychencode.org);
iii. Chromatin interaction mapping, to assess interactions between chromatin state within 200 bp accessible for transcription and other regions of the 3D genome, using data from dorsolateral prefrontal cortex and neural progenitor cells (GSE87112), PsychENCODE, and adult and fetal cortex (73).

Identifying Overlap in Gene Modules between Global and Regional GWAS Results. We quantified the genetic overlap between global area/thickness and each of the brain regions using the human protein interactome from STRING (a database of protein–protein interaction networks) (21) and the genes we identified through MAGMA for each phenotype to create genetic modules for each brain trait. This network-based mapping approach can provide more biologically meaningful information compared to simply looking at overlapping genes between two traits. STRING consists of both physical and functional interactions, derived through co-expression, biological knowledge databases, and computational techniques. Interactions are scored based on accumulation of different types of evidence (21). In our analysis, we used interactions classified as "high confidence" (combined score > 0.7), for the human interaction version 11.0, containing 17,185 proteins and 420,534 interactions (20).

We assessed whether the genes underlying global measures were overlapping or separated from genes underlying regional brain measures (i.e., from GWAS*g+r*) by using a network separation analysis adapted from Menche et al. (20). First, we calculated the mean shortest distance, d_{AB}, between each global (A) and regional brain region (B) pair, as well as the shortest distance between genes within each of the brain phenotype modules (d_{AA} and d_{BB}). To take into account the size of each individual module, we calculated separation (S_{AB}) between global and regional module pairs with the following formula: $S_{AB} = d_{AB} - ((d_{AA} + d_{BB})/2)$. To assess whether global and regional genes demonstrated more significant overlap than expected by chance, 500 random gene sets with network degree-matched genes (i.e., genes with the same number of interactions) as the initial test set were generated to yield a distribution from which test statistics could be calculated from, similar to work from our group (22) and others (20). In addition to using gene lists generated by MAGMA, we also computed separation statistics using genes mapped by FUMA, which includes intergenic mapping (Datasets S18–S20). Visualization of results was done through Cytoscape (24), and functional profiling was completed with g:Profiler (23) (Fig. 1*D*).

Data, Materials, and Software Availability. All data needed to evaluate the conclusions in the paper are present in the paper and/or the *SI Appendix*. UKB data were provided by the public UK Biobank resource. All researchers who wish to access the research resource must register with UK Biobank by completing the registration form in the Access Management System (https://www.ukbiobank.ac.uk/enable-your-research/register). ABCD Study data (https://abcdstudy.org) were processed from the raw structural imaging data held in the NDA. The ABCD data repository grows and changes over time. The ABCD data used in this report came from ABCD Collection Release 2.0.1, which can be found as an NDA Study with DOI: 10.15154/1504041 (74). Brain imaging phenotypes derived from this collection can be found in the NDA Study with DOI: 10.15154/1523026 (75). Imaging and genomics data were taken from participants of the UKB population cohort, obtained from the data repository under accession number 27412 (76).

ACKNOWLEDGMENTS. We would like to thank the research participants and staff involved in data collection of the UK Biobank and Adolescent Brain Cognitive Development (ABCD) Study data. We would also like to thank Tobias Kaufmann for his help processing UK Biobank imaging data. The ABCD Study is a multisite, longitudinal study designed to recruit more than 10,000 children ages 9 and 10 and follow them over 10 y into early adulthood. The ABCD Study is supported by the NIH and additional federal partners under award numbers U01DA041048, U01DA050989, U01DA051016, U01DA041022, U01DA051018, U01DA051037, U01DA050987, U01DA041174, U01DA041106, U01DA041117, U01DA041028, U01DA041134, U01DA050988, U01DA051039, U01DA041156, U01DA041025, U01DA041120, U01DA051038, U01DA041148, U01DA041093, U01DA041089, U24DA041123, and U24DA041147. A full list of supporters is available at https://abcdstudy.org/federal-partners.html. A listing of participating sites and a complete listing of the study investigators can be found at https://abcdstudy.org/study-sites/. ABCD consortium investigators designed and implemented the study and/or provided data but did not necessarily all participate in analysis or writing of this report. This manuscript reflects the views of the authors and may not reflect the opinions or views of the NIH or ABCD consortium investigators. This research was supported by the following funding agencies: NIH R01MH118281 (C.-H.C.) NIH R56AG061163 (C.-H.C.) Canadian Institutes of Health Research and the Kavli Institute for Brain and Mind (C.M.) National Health and Medical Research Council (1113400) and the Australian Research Council (FT180100186 and FL180100072) (P.M.V. and J.Y.) Westlake Education Foundation (J.Y.) Research Council of Norway (project #276082) (D.v.d.M.).

Author affiliations: [a]Department of Radiology, University of California San Diego, La Jolla, CA 92093; [b]School of Statistics, East China Normal University, Shanghai 20050, China; [c]Norwegian Centre for Mental Disorders Research Centre, Division of Mental Health and Addiction, University of Oslo, Oslo 0450, Norway; [d]Division of Biostatistics and Bioinformatics, University of California San Diego, La Jolla, CA 92093; [e]Institute for Molecular Bioscience, The University of Queensland, Brisbane, QLD 4072, Australia; and [f]School of Life Sciences, Westlake University, Hangzhou, Zhejiang 310024, China

1. P. Rakic, Evolution of the neocortex: A perspective from developmental biology. *Nat. Rev. Neurosci.* **10**, 724–735 (2009).
2. A. M. Winkler *et al.*, Joint analysis of cortical area and thickness as a replacement for the analysis of the volume of the cerebral cortex. *Cereb. Cortex* **28**, 738–749 (2018).
3. D. C. Van Essen, C. J. Donahue, M. F. Glasser, Development and evolution of cerebral and cerebellar cortex. *Brain Behav. Evol.* **91**, 158–169 (2018).
4. C. J. Donahue, M. F. Glasser, T. M. Preuss, J. K. Rilling, D. C. Van Essen, Quantitative assessment of prefrontal cortex in humans relative to nonhuman primates. *Proc. Natl. Acad. Sci. U.S.A.* **115**, E5183–E5192 (2018).
5. P. K. Reardon *et al.*, Normative brain size variation and brain shape diversity in humans. *Science* **360**, 1222–1227 (2018).
6. C. Modenato *et al.*, Lessons learned from neuroimaging studies of copy number variants: A systematic review. *Biol. Psychiat.* **90**, 596–610 (2021).
7. L. T. Eyler *et al.*, A comparison of heritability maps of cortical surface area and thickness and the influence of adjustment for whole brain measures: A magnetic resonance imaging twin study. *Twin Res. Hum. Genet.* **15**, 304–314 (2012).
8. J. Shin *et al.*, Global and regional development of the human cerebral cortex: Molecular architecture and occupational aptitudes. *Cereb. Cortex* **30**, 4121–4139 (2020).

9. C. R. Cadwell, A. Bhaduri, M. A. Mostajo-Radji, M. G. Keefe, T. J. Nowakowski, Development and arealization of the cerebral cortex. *Neuron* **103**, 980–1004 (2019).
10. C.-H. Chen *et al.*, Hierarchical genetic organization of human cortical surface area. *Science* **335**, 1634–1636 (2012).
11. C.-H. Chen *et al.*, Genetic topography of brain morphology. *Proc. Natl. Acad. Sci. U.S.A.* **110**, 17089–17094 (2013).
12. C. Makowski *et al.*, Discovery of genomic loci of the human cerebral cortex using genetically informed brain atlases. *Science* **375**, 522–528 (2022).
13. M. Vidal, M. E. Cusick, A.-L. Barabási, Interactome networks and human disease. *Cell* **144**, 986–998 (2011).
14. A. M. Dale, B. Fischl, M. I. Sereno, Cortical surface-based analysis. I. Segmentation and surface reconstruction. *Neuroimage* **9**, 179–194 (1999).
15. S. Purcell *et al.*, PLINK: A tool set for whole-genome association and population-based linkage analyses. *Am. J. Hum. Genet.* **81**, 559–575 (2007).
16. E. Sjöstedt *et al.*, An atlas of the protein-coding genes in the human, pig, and mouse brain. *Science* **367**, eaay5947 (2020).
17. K. L. Grasby *et al.*, The genetic architecture of the human cerebral cortex. *Science* **367**, eaay6690 (2020).
18. S. M. Blazejewski *et al.*, Rpsa signaling regulates cortical neuronal morphogenesis via its ligand, PEDF, and plasma membrane interaction partner, Itga6. *Cereb. Cortex* **32**, 770–795 (2021).
19. Q. Peng *et al.*, Conservation of distinct genetically-mediated human cortical pattern. *PLoS Genet.* **12**, e1006143 (2016).
20. J. Menche *et al.*, Disease networks. Uncovering disease-disease relationships through the incomplete interactome. *Science* **347**, 1257601 (2015).
21. D. Szklarczyk *et al.*, STRING v11: Protein-protein association networks with increased coverage, supporting functional discovery in genome-wide experimental datasets. *Nucleic Acids Res.* **47**, D607–D613 (2019).
22. K. Kauppi *et al.*, Revisiting antipsychotic drug actions through gene networks associated with schizophrenia. *Am. J. Psychiatry* **175**, 674–682 (2018).
23. U. Raudvere *et al.*, g:Profiler: A web server for functional enrichment analysis and conversions of gene lists. *Nucleic Acids Res.* **47**, W191–W198 (2019).
24. P. Shannon *et al.*, Cytoscape: A software environment for integrated models of biomolecular interaction networks. *Genome Res.* **13**, 2498–2504 (2003).
25. J. Yang *et al.*, Conditional and joint multiple-SNP analysis of GWAS summary statistics identifies additional variants influencing complex traits. *Nat. Genet.* **44**, S1–S3 (2012).
26. M. Hawrylycz *et al.*, Canonical genetic signatures of the adult human brain. *Nat. Neurosci.* **18**, 1832–1844 (2015).
27. H. J. Kang *et al.*, Spatio-temporal transcriptome of the human brain. *Nature* **478**, 483–489 (2011).
28. A. Bernard *et al.*, Transcriptional architecture of the primate neocortex. *Neuron* **73**, 1083–1099 (2012).
29. C. L. Hartl *et al.*, Coexpression network architecture reveals the brain-wide and multiregional basis of disease susceptibility. *Nat. Neurosci.* **24**, 1313–1323 (2021).
30. E. Koch, B. Rosenthal, A. Lundquist, C.-H. Chen, K. Kauppi, Interactome overlap between schizophrenia and cognition. *Schizophr. Res.* **222**, 167–174 (2020).
31. C. Makowski, H. Wang, C.-H. Chen, Clinical opportunity awaits at the intersection of genomics and brain imaging. *J. Psychiatry Neurosci.* **47**, E293–E298 (2022).
32. D. van der Meer *et al.*, Quantifying the polygenic architecture of the human cerebral cortex: Extensive genetic overlap between cortical thickness and surface area. *Cereb. Cortex* **30**, 5597–5603 (2020).
33. P. Rakic, A. E. Ayoub, J. J. Breunig, M. H. Dominguez, Decision by division: Making cortical maps. *Trends Neurosci.* **32**, 291–301 (2009).
34. H. Aschard, B. J. Vilhjálmsson, A. D. Joshi, A. L. Price, P. Kraft, Adjusting for heritable covariates can bias effect estimates in genome-wide association studies. *Am. J. Hum. Genet.* **96**, 329–339 (2015).
35. P. A. Garay, A. K. McAllister, Novel roles for immune molecules in neural development: Implications for neurodevelopmental disorders. *Front. Synaptic. Neurosci.* **2**, 136 (2010).
36. V. A. Macht, Neuro-immune interactions across development: A look at glutamate in the prefrontal cortex. *Neurosci. Biobehav. Rev.* **71**, 267–280 (2016).
37. N. Gogtay *et al.*, Dynamic mapping of human cortical development during childhood through early adulthood. *Proc. Natl. Acad. Sci. U.S.A.* **101**, 8174–8179 (2004).
38. B. Kolb *et al.*, Experience and the developing prefrontal cortex. *Proc. Natl. Acad. Sci. U.S.A.* **109**, 17186–17193 (2012).
39. L. A. O'Neill, C. Kaltschmidt, NF-kappa B: A crucial transcription factor for glial and neuronal cell function. *Trends Neurosci.* **20**, 252–258 (1997).
40. M. Michel, M. J. Schmidt, K. Mirnics, Immune system gene dysregulation in autism and schizophrenia. *Dev. Neurobiol.* **72**, 1277–1287 (2012).
41. C. Estrada, A. Villalobo, "Epidermal growth factor receptor in the adult brain" in *The Cell Cycle in the Central Nervous System*, D. Janigro, Ed. (Humana Press, 2006), pp. 265–277.
42. C. T. Primiani *et al.*, Coordinated gene expression of neuroinflammatory and cell signaling markers in dorsolateral prefrontal cortex during human brain development and aging. *PLoS One* **9**, e110972 (2014).
43. K. Brose *et al.*, Slit proteins bind Robo receptors and have an evolutionarily conserved role in repulsive axon guidance. *Cell* **96**, 795–806 (1999).
44. M. Murphy, S. S. Chatterjee, S. Jain, M. Katari, R. DasGupta, TCF7L1 modulates colorectal cancer growth by inhibiting expression of the tumor-suppressor gene EPHB3. *Sci. Rep.* **6**, 28299 (2016).
45. J.-S. Chen *et al.*, PIK3CD induces cell growth and invasion by activating AKT/GSK-3β/β-catenin signaling in colorectal cancer. *Cancer Sci.* **110**, 997–1011 (2019).
46. S. L. Valk *et al.*, Shaping brain structure: Genetic and phylogenetic axes of macroscale organization of cortical thickness. *Sci. Adv.* **6**, eabb3417 (2020).
47. Z. Zhu *et al.*, Integration of summary data from GWAS and eQTL studies predicts complex trait gene targets. *Nat. Genet.* **48**, 481–487 (2016).
48. J. Nasser *et al.*, Genome-wide enhancer maps link risk variants to disease genes. *Nature* **593**, 238–243 (2021).
49. D. J. Schaid, W. Chen, N. B. Larson, From genome-wide associations to candidate causal variants by statistical fine-mapping. *Nat. Rev. Genet.* **19**, 491–504 (2018).
50. S. M. Smith *et al.*, An expanded set of genome-wide association studies of brain imaging phenotypes in UK Biobank. *Nat. Neurosci.* **24**, 737–745 (2021).
51. F. Alfaro-Almagro *et al.*, Confound modelling in UK Biobank brain imaging. *Neuroimage* **224**, 117002 (2021).
52. D. van der Meer *et al.*, Understanding the genetic determinants of the brain with MOSTest. *Nat. Commun.* **11**, 3512 (2020).
53. A. A. Shadrin *et al.*, Vertex-wise multivariate genome-wide association study identifies 780 unique genetic loci associated with cortical morphology. *Neuroimage* **244**, 118603 (2021).
54. D. van der Meer *et al.*, The genetic architecture of human cortical folding. *Sci. Adv.* **7**, eabj9446 (2021).
55. C. E. Palmer *et al.*, Distinct regionalization patterns of cortical morphology are associated with cognitive performance across different domains. *Cereb. Cortex* **31**, 3856–3871 (2021).
56. L. T. Elliott *et al.*, Genome-wide association studies of brain imaging phenotypes in UK Biobank. *Nature* **562**, 210–216 (2018).
57. C. Sudlow *et al.*, UK biobank: An open access resource for identifying the causes of a wide range of complex diseases of middle and old age. *PLoS Med.* **12**, e1001779 (2015).
58. K. L. Miller *et al.*, Multimodal population brain imaging in the UK Biobank prospective epidemiological study. *Nat. Neurosci.* **19**, 1523–1536 (2016).
59. C. Bycroft *et al.*, The UK Biobank resource with deep phenotyping and genomic data. *Nature* **562**, 203–209 (2018).
60. N. D. Volkow *et al.*, The conception of the ABCD study: From substance use to a broad NIH collaboration. *Dev. Cognit. Neurosci.* **32**, 4–7 (2018).
61. K. A. Uban *et al.*, Biospecimens and the ABCD study: Rationale, methods of collection, measurement and early data. *Dev. Cognit. Neurosci.* **32**, 97–106 (2018).
62. B. Fischl *et al.*, Whole brain segmentation: Automated labeling of neuroanatomical structures in the human brain. *Neuron* **33**, 341–355 (2002).
63. H. Akaike, A new look at the statistical model identification. *IEEE Trans. Automat. Contr.* **19**, 716–723 (1974).
64. G. Schwarz, Estimating the dimension of a model. *Ann. Stat.* **6**, 461–464 (1978).
65. R. Tibshirani, The lasso method for variable selection in the Cox model. *Stat. Med.* **16**, 385–395 (1997).
66. G. Abraham, M. Inouye, Fast principal component analysis of large-scale genome-wide data. *PLoS One* **9**, e93766 (2014).
67. L. Jiang *et al.*, A resource-efficient tool for mixed model association analysis of large-scale data. *Nat. Genet.* **51**, 1749–1755 (2019).
68. B. K. Bulik-Sullivan *et al.*, LD Score regression distinguishes confounding from polygenicity in genome-wide association studies. *Nat. Genet.* **47**, 291–295 (2015).
69. K. Watanabe, E. Taskesen, A. van Bochoven, D. Posthuma, Functional mapping and annotation of genetic associations with FUMA. *Nat. Commun.* **8**, 1826 (2017).
70. C. A. de Leeuw, J. M. Mooij, T. Heskes, D. Posthuma, MAGMA: Generalized gene-set analysis of GWAS data. *PLoS Comput. Biol.* **11**, e1004219 (2015).
71. C. Chelala, A. Khan, N. R. Lemoine, SNPnexus: A web database for functional annotation of newly discovered and public domain single nucleotide polymorphisms. *Bioinformatics* **25**, 655–661 (2009).
72. D. Wang *et al.*, Comprehensive functional genomic resource and integrative model for the human brain. *Science* **362**, aat8464 (2018).
73. P. Giusti-Rodríguez *et al.*, Using three-dimensional regulatory chromatin interactions from adult and fetal cortex to interpret genetic results for psychiatric disorders and cognitive traits. biorxiv [Preprint] (2019). https://doi.org/10.1101/406330 (Accessed 14 March 2022).
74. T. Jernigan *et al.*, Data from "Adolescent Brain Cognitive Development Study (ABCD) 2.0.1 release." The National Institute of Mental Health Data Archive (NDA). https://doi.org/10.15154/1504041. Accessed 1 November 2019.
75. C. Makowski *et al.*, Data from "Discovery of genomic loci of the human cerebral cortex using genetically informed brain atlases." The National Institute of Mental Health Data Archive (NDA). https://doi.org/10.15154/152302. Deposited 24 January 2022.
76. O. Andreassen *et al.*, Data from Project "Boosting the power of GWAS using novel statistical tools". *UK Biobank*. https://www.ukbiobank.ac.uk/enable-your-research/approved-research/boosting-the-power-of-gwas-using-novel-statistical-tools. Accessed 1 November 2019.